Available online at www.sciencedirect.com
SCIENCE DIRECT®
Journal of Solid State Chemistry 177 (2004) 2881–2888
JOURNAL OF SOLID STATE CHEMISTRY
http://elsevier.com/locate/jssc

$(La_{0.4}Ba_{0.4}Ca_{0.2})(Mn_{0.4}Ti_{0.6})O_3$: A new titano-manganate with a high dielectric constant and antiferromagnetic interactions

Pika Jha,[a] Sarita Rai,[a] Kandalam V. Ramanujachary,[b] Samuel E. Lofland,[b] and Ashok K. Ganguli[a,*]

[a] *Department of Chemistry, Indian Institute of Technology, Hauz Khas, New Delhi 110016, India*
[b] *Department of Chemistry and Physics, Rowan University, Glasboro, NJ, USA*

Received 17 January 2004; received in revised form 26 April 2004; accepted 2 May 2004

Abstract

A new perovskite-based titano-manganate, $(La_{0.4}Ba_{0.4}Ca_{0.2})(Mn_{0.4}Ti_{0.6})O_3$, has been prepared by the ceramic route at 1100°C. This oxide was found to possess the cubic perovskite structure with 'a' = 3.9477(23) Å (space group $Pm\bar{3}m$). The refined composition as obtained by Rietveld analysis of powder X-ray data was found to be $(La_{0.44}Ba_{0.38}Ca_{0.18})(Mn_{0.43}Ti_{0.57})O_{2.91(3)}$ ($R_p = 0.0704$, w$R_p = 0.0828$). The composition was also ascertained by Energy dispersive X-ray analysis. Iodometric studies led to a slightly higher oxygen content (compared to Rietveld refinement) corresponding to an average manganese oxidation state of 3.05. The above oxide was found to exhibit high dielectric constant (ε) of 6980 at 1 kHz decreasing to 590 at 100 kHz. At high temperatures (200°C) it shows an unusually high dielectric constant of 20,000 at 1 kHz. In addition to the dielectric properties, detailed magnetic studies show evidence of long-range antiferromagnetic interactions near 5 K. The presence of unusually high dielectric constant coupled with the long-range magnetic interactions may open up interesting applications.

Keywords: Perovskite; Oxides; Magnetic properties; Dielectric properties

1. Introduction

Currently there is a major thrust in the design of new materials with high dielectric constant and low loss. Several new materials have been found to show promising dielectric properties like high dielectric constant and stable dielectric properties with respect to frequency and temperature variation. Traditionally, materials comprising ions with closed shell (d^0) electronic configuration are known to have interesting dielectric properties (e.g., oxides of Ti^{4+}, Nb^{5+} and Ta^{5+}). The interest in the dielectric materials stem from their large scale use in the electronic industry including microwave communication systems in which they serve as dielectric resonators. Hence, there is tremendous activity towards discovering new dielectric materials [1–8]. In the recent past, there have been studies [9–11] on $CaCu_3Ti_4O_{12}$, which show an unusually high dielectric constant (greater than 1000). Recently, we reported synthesis of $Nd_2Ba_2CaZn_2Ti_3O_{14}$ [12], which shows a high dielectric constant of 59 at 100 kHz. Analogous oxides of La and Pr also show high dielectric constant (70 and 57, respectively) [13].

A variety of oxides showing interesting magnetic properties belong to the perovskite structure. Among the various magnetic perovskite oxides, the rare earth manganates are of great importance, since they can exhibit a plethora of properties and phenomena, which are highly dependent on various factors like cation size, pressure, magnetic and electrical fields. Oxides based on $LaMnO_3$ [14], are well-known for their ferromagnetic behavior as well for their giant-magnetoresistance. Oxides in which the A site (i.e., La) has been substituted with other cations like Ca or Pb are also found to show ferromagnetism and magnetoresistance. For example, oxides like $La_{0.7}Ca_{0.3}MnO_3$ [15], show electron spin ordering along with magnetoresistance. The parent

*Corresponding author. Fax: +91-11-26854715.
E-mail address: ashok@chemistry.iitd.ernet.in (A.K. Ganguli).

0022-4596/$ - see front matter © 2004 Elsevier Inc. All rights reserved.
doi:10.1016/j.jssc.2004.05.009

compound $LaMnO_3$ is antiferromagnetic, but substitution with other metal ions, e.g., Sr allows hopping of e_g electrons belonging to Mn^{+3} to the neighboring sites containing Mn^{+4} ions. This introduces a long-range ferromagnetic spin ordering through the double exchange mechanism. The perovskite oxides of the type $Ln_{1-x}A_xMnO_3$ are especially interesting because they show long-range ordering of the Mn^{+3} ($t_{2g}^3e_g^1$) and Mn^{+4} ($t_{2g}^3e_g^0$) ions which is linked to the antiferromagnetic spin ordering. The magnetic properties of $La_{1-x}Ca_xMnO_3$ perovskites with $x = 0.6$ and 0.8 were reported [16] over a large temperature range. A transition from mictomagnetic to antiferromagnetic state is evidenced at low temperatures for the samples with high lanthanum content. As the calcium content increases a essentially predominantly antiferromagnetic behavior is observed.

In this paper we report a new oxide, $(La_{0.4}Ba_{0.4}Ca_{0.2})(Mn_{0.4}Ti_{0.6})O_{3.015}$ based on $LaMnO_3$ where a high concentration of Ti is substituted in the *B*-site of the perovskite. Our recent studies on similar zinc based systems [12,13] and their encouraging dielectric properties have prompted us to substitute the Zn site with Mn, in order to observe the effect of the magnetic ion in the *B*-site on the dielectric properties of the oxide. Till date the studies on perovskites containing Mn and Ti in the *B*-sites is restricted to a maximum of 30% of Ti [17]. It is found that substitution of tetravalent Ti instead of Mn^{4+} suppresses the ferromagnetism and double exchange mechanism, and favors intragrain spin fluctuation. In the oxide $(La_{0.4}Ba_{0.4}Ca_{0.2})(Mn_{0.4}Ti_{0.6})O_3$, 60% of the *B*-sites are occupied by titanium. Our aim is to design a bi-functional material with unusual dielectric and magnetic properties and to see the effect of increased concentration of Ti^{4+} ions in the *B*-site on the dielectric and magnetic properties of the oxide. We discuss the synthesis, structural analysis by Rietveld refinement, magnetic properties and also the frequency and temperature-dependent dielectric properties of this oxide.

2. Experimental

$La_{0.4}Ba_{0.4}Ca_{0.2}Mn_{0.4}Ti_{0.6}O_3$ was prepared by the ceramic method. Stoichiometric amounts of La_2O_3, TiO_2, $CaCO_3$, $BaCO_3$ and $MnCO_3$ were taken. The rare-earth oxides were dried at 900°C for 6 h before weighing, while the other oxides and carbonates were dried at 150°C. The reactants were thoroughly mixed in an agate mortar and heated in alumina boats at 900°C for 12 h and 1025°C for 48 h followed by heating at 1100°C for 40 h with intermittent grinding. The resulting powder was ground, mixed with 5% PVA (polyvinyl alcohol) solution and compacted into pellets at a pressure of 4 tons. The pellets were then sintered at 1100°C for 3 h. Powder X-ray diffraction was carried out after each step with a Bruker D8 Advance diffractometer with Cu$K\alpha$ radiation. A step size of 0.05° in 2θ with step time of 1 s was used for the 2θ range of 10–70°. The raw data was subjected to background correction and $K_{\alpha 2}$ stripping. Lattice parameters were refined by a least squares fit of the observed *d*-values. For Rietveld analysis a step size of 0.02 and a step time of 6 s was used. Refinement was carried out using the GSAS software [10]. Standard procedure was followed for the refinement. The La, Ba and Ca ions were statistically allocated to the 1*a* site with 100% occupancy in the fixed ratio of 0.44:0.38:0.18, which was close to the composition obtained by EDX. The titanium ions and the transition metal ions were statistically allocated to the 1*b* site with 100% occupancy in the fixed ratio of 0.57:0.43. The final refinement cycle consisted of variables including the cell parameter, scale factor, the zero point correction, the absorption correction, the profile, six terms of the background fitting polynomial (shifted Chebyshev) and the isotropic thermal parameters. Oxygen site occupancy was refined as well.

Electron diffraction studies were carried out on a JEOL 2010F transmission electron microscope operating at 200 kV. The oxide was dispersed in ethanol and then mounted on holey carbon grids.

Scanning electron micrographs (SEM) were obtained on sintered disks with a Cambridge Stereoscan 360 electron microscope. Energy dispersive analysis of X-rays (EDX) has been carried out on a LEO 4401 electron microscope by integrating it with an Oxford ISIS EDX system. The error associated with the compositions obtained by EDX measurements is 0.01. The oxygen content was estimated using iodometric titration. 80 mg of the sample was dissolved in concentrated HCl. Standard procedure was followed for the estimation, and the liberated iodine was titrated with sodium thiosulfate solution, which was standardized using standard potassium dichromate solution. XPS measurements were performed on a Perkin Elmer (model 1257) X-ray Photoelectron spectrometer operating at a base pressure of 6×10^{-10} Torr. From the dual anode X-ray source Mg$K\alpha$ (1253.6 eV) line was used. The spectra of the samples were recorded before and after sputtering at the top surface. Argon ion bombardment was done by a differentially pumped ion gun. The sputtering of the sample was carried out by a 3 keV argon beam, at a pressure of 10^{-8} Torr for 2 min. The binding energy (E_b) is calibrated with respect to the peak position of the C 1*s* core level. The XPS wide scan was acquired using a 100 eV pass energy at a step of 1.0 eV and XPS C 1*s* core level spectra was acquired at 0.05 eV step with a pass energy of 40 eV.

Magnetic data were collected with a Quantum Design, Physical Property Measuring System (PPMS) in the

temperature range 5–300 K. Both cooling and warming studies were carried out. The samples were first cooled in fields of 10 kOe. The effective magnetic moment (μ), assuming spin only contribution was obtained from the slope of the high temperature region in the inverse susceptibility vs. temperature plot. The magnetic susceptibility was corrected for diamagnetic contribution of the ions using the values of Selwood [18].

The dielectric constant was measured on disks coated with silver using a HP 4284L LCR meter in the frequency range of 50–500 kHz. Measurements of the dielectric constant and dielectric loss was carried out by varying the temperature in the range 35–300°C. The density of the sintered disks was estimated by the Archimedes method using CCl_4 as the solvent. The disks were soaked in the organic medium for 36 h and weights were taken till a constant weight was observed. For consistency, three different density measurements were carried out for each sample. The actual density was found to vary between 92% and 94% of theoretical density.

3. Results and discussions

The powder X-ray diffraction studies shows the formation of the cubic phase of $La_{0.4}Ba_{0.4}Ca_{0.2}Mn_{0.4}Ti_{0.6}O_3$, along with presence of reactants as impurity phases at 900°C. The amounts of impurities were observed to diminish with higher heat treatments. At 1025°C, some amount of manganese oxide and some $BaTiO_3$, are observed together with the product phase. A final heating at 1100°C lead to the formation of X-ray pure $La_{0.4}Ba_{0.4}Ca_{0.2}Mn_{0.4}Ti_{0.6}O_3$. The diffraction pattern could be indexed based on a cubic cell (Fig. 1) with the lattice parameter of 'a' = 3.9261(4) Å. Rietveld refinement was carried out on the sample after the final heating stage. The exact procedure followed for the refinement is outlined in Section 2. The structure refined to reasonable R-values in the space group $Pm\bar{3}m$. The lattice parameters obtained from Rietveld refinement was 3.9477(23). The region corresponding to 28.74–29.28 in 2θ was excluded since reflections corresponding to impurity phase was present in this region. This impure phase was not detectable in the normal powder X-ray diffraction pattern (fast scan) as shown in Fig. 1. The final refined composition was $(La_{0.44}Ba_{0.38}Ca_{0.18})(Mn_{0.43}Ti_{0.57})O_{2.91(3)}$. The metal occupancies were fixed according to the values obtained from EDX results. Refining the metal occupancies did not result in improved refinement. The final refined values of isotropic thermal factors, occupancies and Wyckoff symbols for this composition are listed in Table 1. The observed, calculated and the difference plot is shown in Fig. 2.

Thus the oxide has a mixture of cations at the 'A' and 'B' sites of the perovskite ABO_3. We have not found any indication of the ordering of A or B ions in perovskite structure as reported earlier [19,20]. The lack of cationic order in the present compound seems to be consistent with our earlier reports on the related oxide $Nd_2Ba_2CaZn_2Ti_3O_{14}$ [12]. The copper and lanthanum-based oxide $La_2Ba_2CaCu_2Ti_3O_{14}$ was also reported to have the disordered cubic structure [20]. Note that electron diffraction studies on $La_{0.4}Ba_{0.4}Ca_{0.2}Mn_{0.4}Ti_{0.6}O_3$ show the cubic reciprocal lattice as expected for a disordered perovskite lattice (Fig. 3).

Scanning electron micrograph (SEM) for the title oxide has been obtained from the pellets compacted at 8 ton pressure. It is seen that the material has few pores (Fig. 4(a)). The grains have an average size of 0.5 μm and are spherical in shape, and have well-defined grain boundaries. EDX analysis of the oxide was carried out to determine the exact composition. It was found that the composition was $La_{0.44(1)}Ba_{0.4(1)}Ca_{0.19(1)}Mn_{0.33(1)}Ti_{0.57(1)}O_3$. The EDX spectrum is shown in Fig. 4(b). Note that in the Rietveld refinement the total occupancy of Mn and Ti at the B site of the ABO_3 structure was fixed to 1.00 which led to the composition $(La_{0.44}Ba_{0.38}Ca_{0.18})(Mn_{0.43}Ti_{0.57})O_{2.91(3)}$. This is very close to the nominal composition of $(La_{0.4}Ba_{0.4}Ca_{0.2})(Mn_{0.4}Ti_{0.6})O_3$. Thus the EDX data suggests a small Mn-deficiency in the compound. Iodometric titration was carried out to estimate the amount of Mn^{4+} of the sample and hence to calculate the total oxygen content. The average manganese oxidation state was 3.05. Thus there is a small amount of manganese in the +4 state. X-ray photoelectron spectroscopy (XPS) of this oxide has been carried out. The peaks corresponding to all the ions have been obtained as shown in Fig. 5(a). The Mn peaks have been obtained at 642.15 and 655.3 eV (Fig. 5(b)), which is close to the value of 642.5 and 654.2 eV of the $2p_{3/2}$ and $2p_{1/2}$ states of Mn^{3+} as reported in standard literature [21]. The peak height ratio of $2p_{1/2}$ to $2p_{3/2}$ is 1.16, which is very close to the expected value of 1.15 for Mn^{3+}.

$(La_{0.4}Ba_{0.4}Ca_{0.2})(Mn_{0.4}Ti_{0.6})O_3$ shows an unusually high dielectric constant of around 6000 at 1 kHz. The high values of the dielectric constant appears to be in line with Koop's theory [22] which has been successfully applied to explain the origin of high dielectric constant (ε) of ferrites [23]. The dielectric structure is supposed to be composed of fairly well conducting grains which are separated by a second thin layer of non-conducting or poorly conducting grain boundaries. A plot of the variation of dielectric constant and dielectric loss as a function of frequency is presented in Fig. 6. It is seen that the dielectric constant decreases sharply with

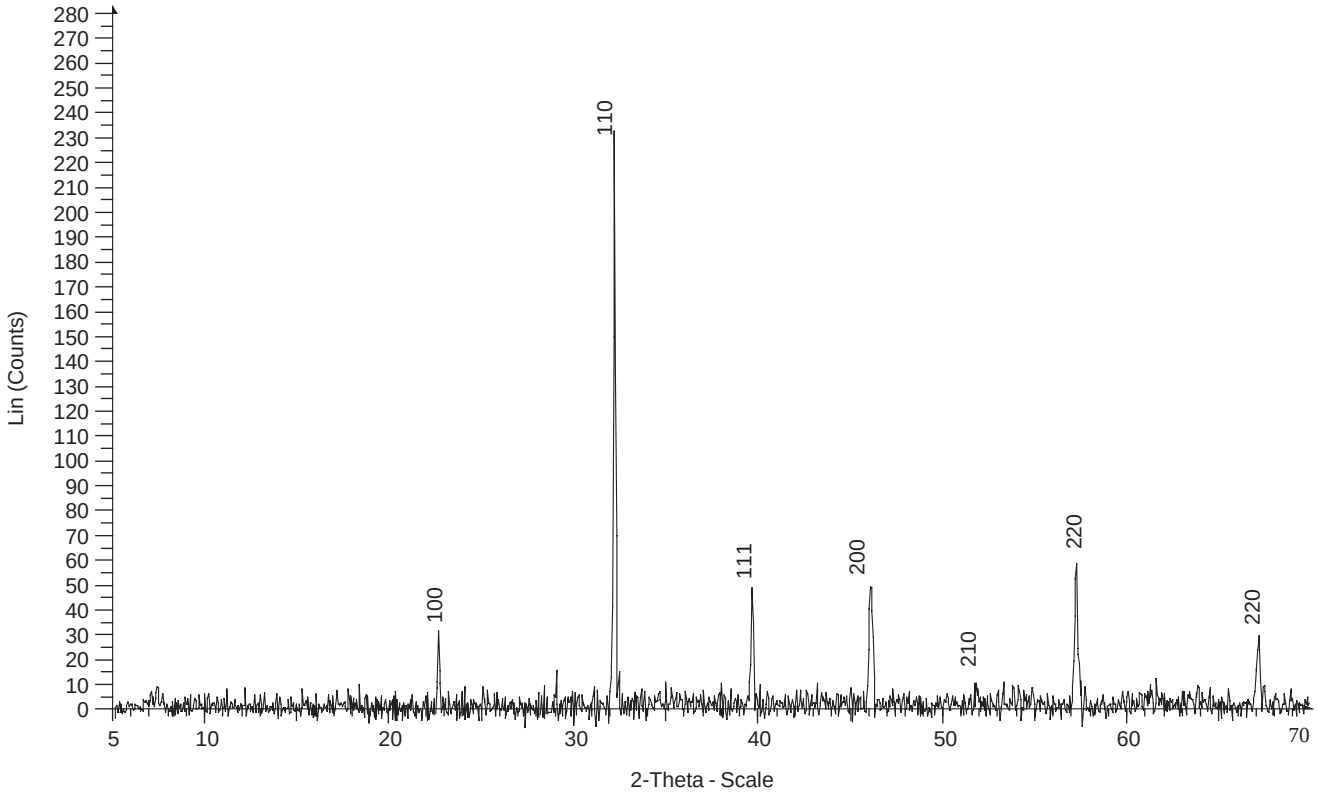

Fig. 1. Powder X-ray diffraction patterns of $(La_{0.4}Ba_{0.4}Ca_{0.2})(Mn_{0.4}Ti_{0.6})O_3$ after sintering at 1100°C.

Table 1
Positional, thermal and occupancy factors of $(La_{0.44}Ba_{0.38}Ca_{0.18})(Mn_{0.43}Ti_{0.57})O_{2.91(3)}$ after refinement of powder X-ray data

Atoms	Wyckoff symbol	Occupancy	x	y	z	$U_{iso} \times 100$
La	1*a*	0.44	0.0	0.0	0.0	0.39(10)
Ba	1*a*	0.38	0.0	0.0	0.0	0.39(10)
Ca	1*a*	0.18	0.0	0.0	0.0	0.39(10)
Mn	1*b*	0.43	0.5	0.5	0.5	0.73(13)
Ti	1*b*	0.57	0.5	0.5	0.5	0.73(13
O	3*c*	0.969(27)	0.0	0.5	0.5	1.39(61)

'*a*' = 3.9477(23), space group $Pm\bar{3}m$; $R(F^2) = 0.035$, $R_p = 0.0704$, $wR_p = 0.0828$.

frequency showing a value of 592 at 100 kHz. Both the dielectric constant and dielectric loss decrease with frequency. The decrease is rapid at intermediate frequencies and becomes sluggish at both higher and lower frequencies. We have found the presence of both Mn^{3+} and Mn^{4+} (from iodometry and XPS) in the above oxide. It is found that 4.2% of the total Mn is present in the tetravalent state, the remaining being in the trivalent state. The decrease in dielectric constant and dielectric loss upon increasing frequency takes place when the hopping rate of the electron exchange between Mn^{3+} and Mn^{4+} ions cannot follow the alternating frequency of the applied field beyond a certain critical frequency [23]. Similar behavior in case of ions in octahedral sites of ferrites have been reported earlier [24,25]. Another reason that could explain this behavior may be that the grain boundaries are effective at lower frequencies. The dielectric loss (D) shows high values of 1.2 over a large temperature range from 5 to 100 kHz. Interestingly this compound was found to show an increase of dielectric constant with temperature and has a value of 8000 at 200°C at 100 kHz (Fig. 7(a)). Similar behavior is also observed at low frequencies and at 1 kHz, the dielectric constant increases from 7000 at room temperature to 20,000 at 200°C (Fig. 7(b)). An increase in dielectric loss is also observed with rise in

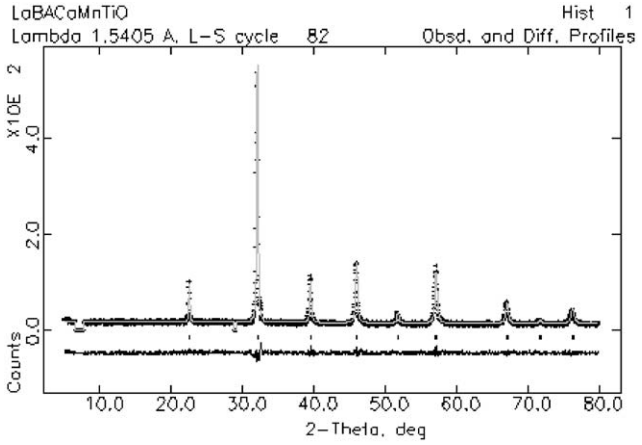

Fig. 2. Observed, calculated and difference pattern of the oxide with composition $(La_{0.44}Ba_{0.38}Ca_{0.18})(Mn_{0.43}Ti_{0.57})O_{2.91(3)}$ as obtained by Rietveld refinement of powder X-ray data.

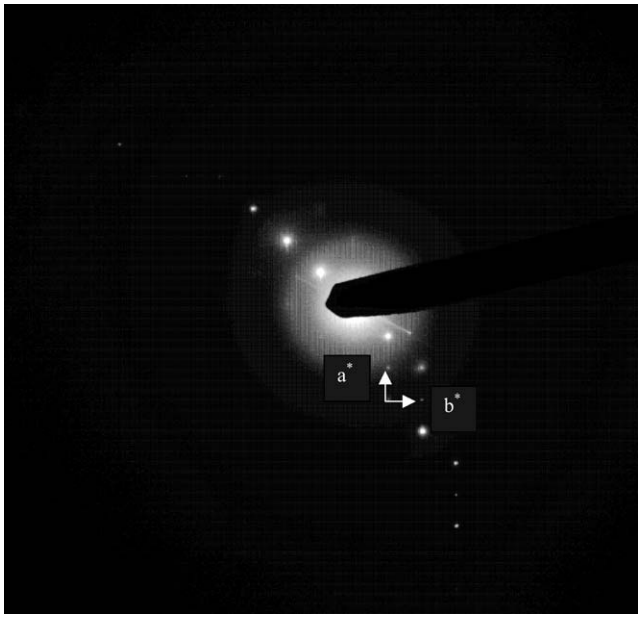

Fig. 3. Electron diffraction pattern of $(La_{0.4}Ba_{0.4}Ca_{0.2})(Mn_{0.4}Ti_{0.6})O_3$.

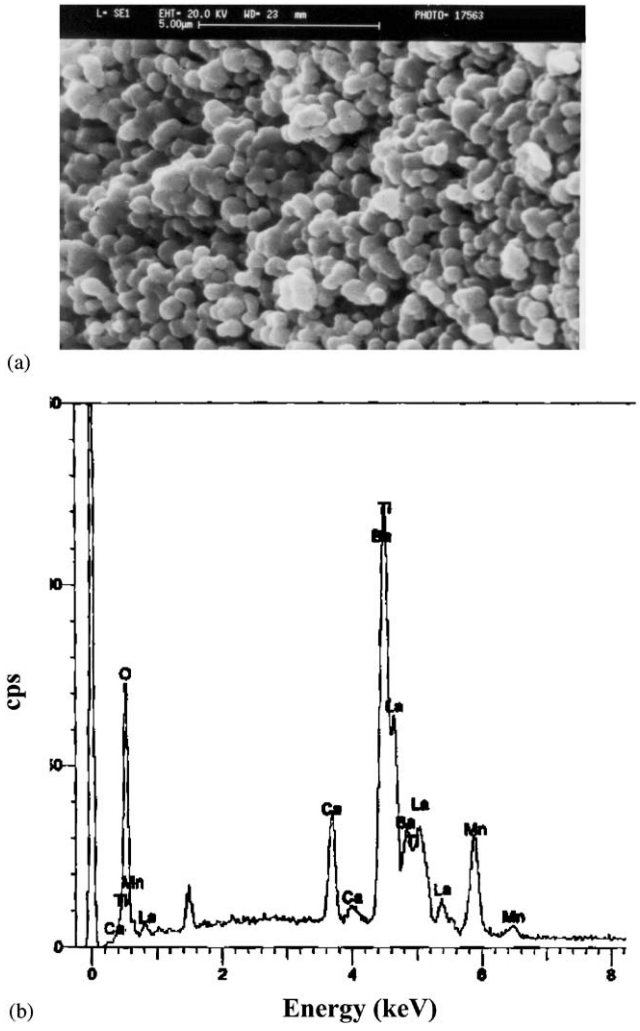

Fig. 4. (a) Scanning electron micrograph and (b) EDX spectrum of $(La_{0.4}Ba_{0.4}Ca_{0.2})(Mn_{0.4}Ti_{0.6})O_3$.

temperature (Figs. 7(a) and (b)). This is probably because of the fact that the electron hopping between adjacent Mn^{3+} and Mn^{4+} is thermally activated, which leads to higher dielectric loss at elevated temperatures. It is possible that the polarization mechanism in this compound is correlated with the electric conduction that occurs primarily by hopping. Therefore the dielectric constant and the dielectric loss increase as the temperature increases. Note that the dielectric constant had a value of 592 at 35°C at 100 kHz.

Apart from the dielectric studies we have also examined the temperature dependent DC magnetic susceptibility of the oxide. The magnetic susceptibility (measured at 10 kOe) of $(La_{0.4}Ba_{0.4}Ca_{0.2})(Mn_{0.4}Ti_{0.6})O_3$ is shown in Fig. 8. The onset of antiferromagnetic interaction at temperatures below 5 K is evident from the plot of χ_M^{-1} (inset of Fig. 8(a)). The susceptibility also shows a steady decrease in the vicinity of 300 K (Figs. 8(a) and (b)). In an effort to understand the higher than expected effective magnetic moment observed in $La_{0.4}Ba_{0.4}Ca_{0.2})(Mn_{0.4}Ti_{0.6})O_3$, we have considered the possible ferromagnetic contribution from the La–*A*–Mn–O (*A* = Ba and/or Ca) pervoskites. It must be noted that no evidence of these phases is detected in the powder X-ray diffraction within the limitation of this technique. However, their contribution to the overall magnetic susceptibility will often lead to overestimated effective magnetic moments. It is well known that alkaline-earth-doped lanthanum manganates can display ferromagnetic order and the so-called colossal magnetoresistance (CMR) that has garnered so much attention of late. To estimate quantitatively the ferromagnetic contribution arising from these phases, we

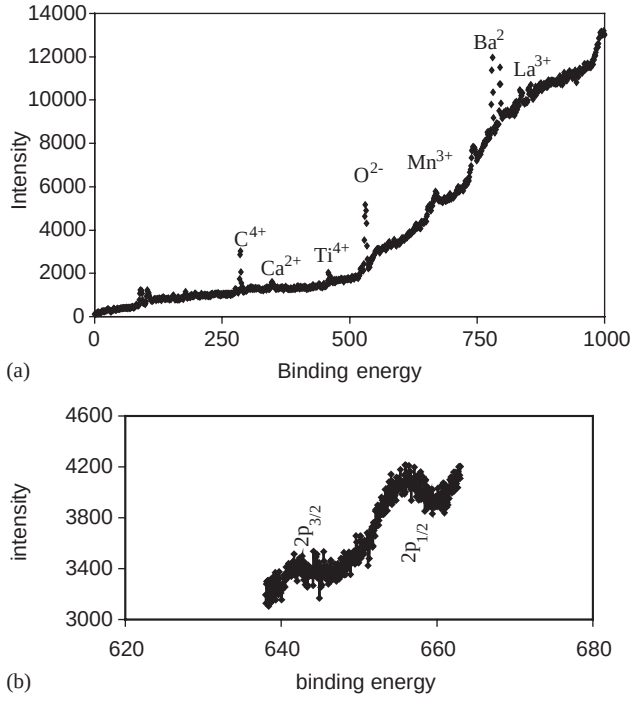

Fig. 5. (a) XPS spectrum of $(La_{0.44}Ba_{0.38}Ca_{0.18})(Mn_{0.43}Ti_{0.57})O_{3.015}$. (b) Enlarged spectrum in the region of 620–680 eV to show the Mn peaks.

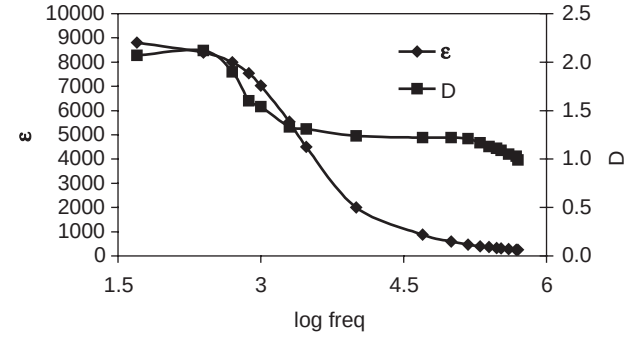

Fig. 6. Plot of variation of dielectric constant and dielectric loss for $(La_{0.4}Ba_{0.4}Ca_{0.2})(Mn_{0.4}Ti_{0.6})O_3$. Measurements were done at room temperature.

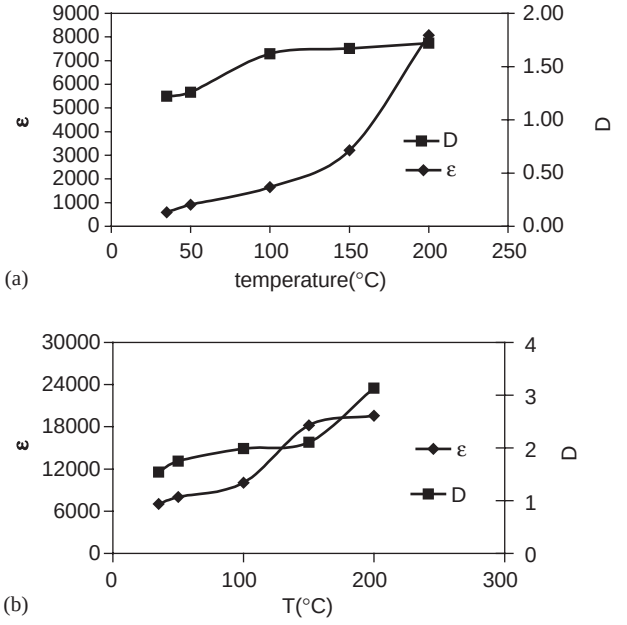

Fig. 7. Plot of variation of dielectric constant and dielectric loss for $(La_{0.4}Ba_{0.4}Ca_{0.2})(Mn_{0.4}Ti_{0.6})O_3$ with temperature at: (a) 100 kHz and (b) 1 kHz.

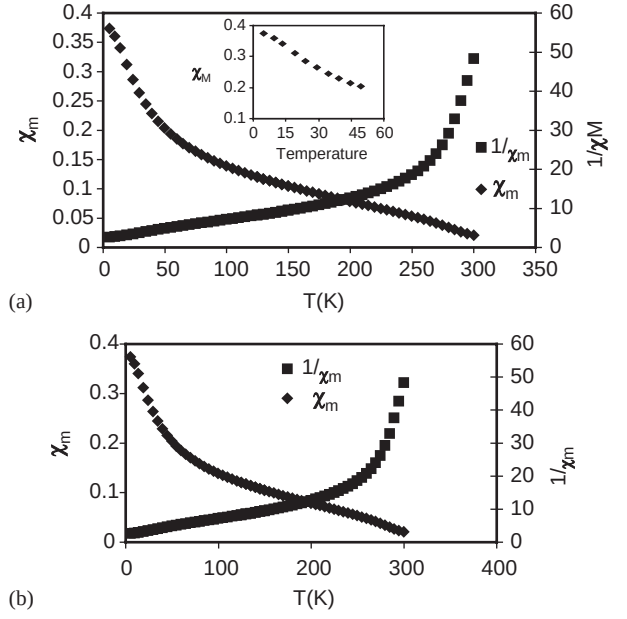

Fig. 8. Plot of variation of χ_M^{-1} and χ_M with temperature for $(La_{0.4}Ba_{0.4}Ca_{0.2})(Mn_{0.4}Ti_{0.6})O_3$ during the (a) cooling cycle. Inset shows the antiferromagnetic transition with a magnified temperature scale; and (b) heating cycle.

have measured the magnetization isotherms at several temperatures. At 250 K (Fig. 9), there is clear evidence of ferromagnetism. Interestingly however, the spontaneous moment is only about 1% of that expected from the 3.5–4 μ_B/Mn reported in the CMR materials [26]. Given the chemical formula, it is seems reasonable to suppose that domains of $La_{1-x}A_xMnO_3$ (A = Ba and/or Ca) may co-exist with the main phase. These domains however have not been seen in our transmission electron microscopy studies which is possible due to the very small amount (magnetic studies indicate $\sim$1% of such domains). The slope of the line fit to the magnetization data between 20 and 50 kOe yields the susceptibility and the intercept corresponds to the spontaneous magnetic moment. The total susceptibility was then corrected for the ferromagnetic impurities and a Curie–Weiss plot of the revised data is shown in Fig. 10. In Fig. 11 we show the evolution of the spontaneous moment as a function of temperature. It turns out that the onset of the ferromagnetism occurs near 300 K, in the vicinity of the Curie temperature of $La_{1-x}Ba_xMnO_3$ for $x \sim 0.2$ [27]. It

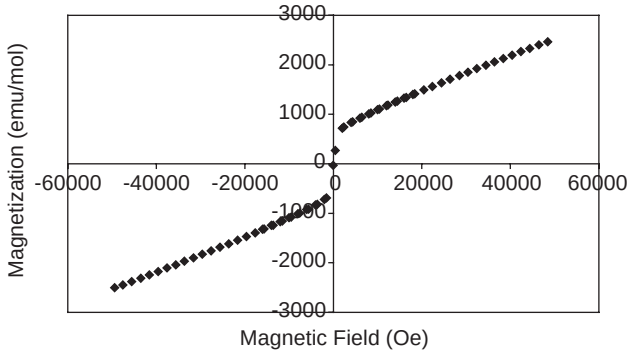

Fig. 9. Field dependent magnetization of $(La_{0.4}Ba_{0.4}Ca_{0.2})(Mn_{0.4}Ti_{0.6})O_3$ at 250 K.

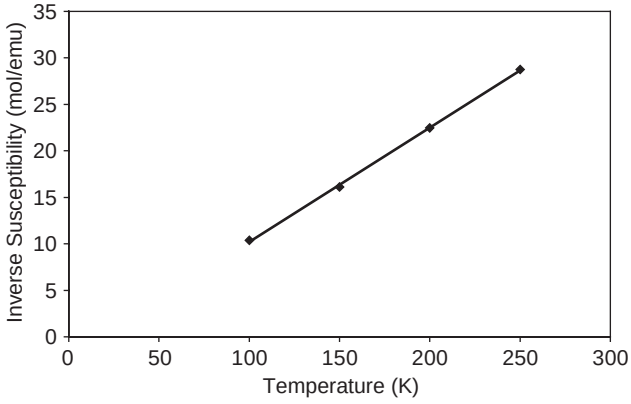

Fig. 10. Inverse magnetic susceptibility corrected for ferromagnetic impurities as a function of temperature.

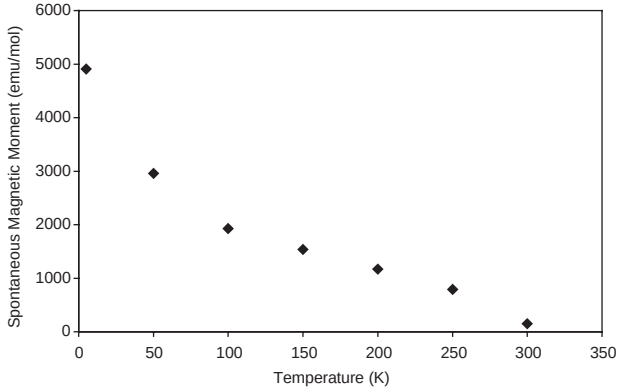

Fig. 11. Variation of the spontaneous magnetic moment of the alkaline earth-doped $LaMnO_3$ pervoskite impurities as a function of temperature.

is likely that there is a range of x values for both Ba and Ca substituted compounds, giving rise to the observed complex temperature dependence to the spontaneous magnetization. The extracted "intrinsic" susceptibility (Fig. 10) yields an effective moment of 5.74 μ_B, much larger than the value of 4.9 μ_B expected from Mn^{3+} ions. However, it must be noted that the "intrinsic" susceptibility determined from the slope is still an overestimated value in view of a large high-field susceptibility of rare earth manganates and also because of the presence of multiple ferromagnetic impurities. The presence of antiferromagnetic interaction coupled with high dielectric constant is unusual in transition-metal-containing oxides, with a few exceptions like $ZnFe_2O_4$ [23,25] and $YMnO_3$ [28,29]. Coupled magnetic and electric domains have been experimentally observed [30] in $YMnO_3$, which is both a ferroelectric and antiferromagnetic oxide. Recently, antiferromagnetic interactions were observed in the compound $CaMn_2O_4$ [31] where it was seen that every Mn^{3+} (d^4) ion has six different superexchange interactions with its neighboring Mn^{3+} ions since all six Mn–O bonds of each MnO_6 octahedron are different because of the Jahn–Teller distortion. The magnetic structure was studied by powder neutron diffraction, which showed that the antiferromagnetic interactions of the Mn–O–Mn depend primarily on the asymmetry and the Mn–O bond length of the Mn–O–Mn linkage, but not on the Mn–O–Mn bond angle. The mechanism of antiferromagnetic interaction in the oxide $(La_{0.4}Ba_{0.4}Ca_{0.2})(Mn_{0.4}Ti_{0.6})O_3$, could be similar to that reported for $CaMn_2O_4$.

The oxide $(La_{0.4}Ba_{0.4}Ca_{0.2})(Mn_{0.4}Ti_{0.6})O_3$ is a novel oxide since it possesses a high dielectric constant as compared to most of the known dielectric materials that have dielectric constant around 30. Very few oxides (other than ferroelectric oxides) show dielectric constant above 40. Apart from the *Ln*–Ba–Ti–O oxides of the type $Ba_{6-3x}(Nd,Bi_y)_{8+2x}Ti_{18}O_{54}$ ($x = 2/3$, $0 < y < 0.2$) [32], recently high dielectric constant has been reported in $CaCu_3Ti_4O_{12}$ [9–11] and $Ln_2Ba_2CaZn_2Ti_3O_{14}$ [12,13] (Ln = La, Pr, and Nd). The high value of the dielectric constant coupled with the magnetic properties of this oxide merits the attention of the electronic industry.

4. Conclusion

We have synthesized for the first time the disordered cubic perovskite oxide $(La_{0.4}Ba_{0.4}Ca_{0.2})(Mn_{0.4}Ti_{0.6})O_3$. This oxide shows antiferromagnetic interaction and also a very high dielectric constant of 592 at 100 kHz, which makes this oxide an interesting material for further study. It also shows a substantial increase (nearly ten-fold) in the dielectric constant at high temperatures (200°C). The high dielectric constant and loss in this oxide especially at elevated temperatures suggest a hopping conduction between Mn^{3+} and Mn^{4+} in this oxide.

Acknowledgments

Financial assistance from CSIR, Govt. of India, is gratefully acknowledged. KVR and SEL thank the High Technology Work Force Grant awarded by the State of New Jersey. We thank National Physical Laboratory, New Delhi, for the XPS data.

References

[1] D. Kolar, D. Suvorov, Eur. J. Solid State Inorg. Chem. 32 (1995) 751.
[2] M.A. Akbas, P.K. Davies, J. Am. Ceram. Soc. 81 (1998) 670.
[3] M.A. Akbas, P.K. Davies, J. Am. Ceram. Soc. 80 (1997) 1727.
[4] R.J. Cava, J. Mater. Chem. 11 (2001) 54.
[5] R.J. Cava, J.J. Krajewski, R.S. Roth, Mater. Res. Bull. 34 (1999) 355.
[6] M. Thirumal, I.N. Jawahar, K.P. Surendran, P. Mohanan, A.K. Ganguli, Mater. Res. Bull. 37 (2002) 185.
[7] H.J. Lee, K.S. Hong, S.J. Kim, I.T. Kim, Mater. Res. Bull. 32 (1997) 847.
[8] Y.J. Wu, X.M. Chen, J. Mater. Res. 16 (2001) 1734.
[9] M.A. Subramanian, D. Li, N. Duan, B.A. Reisner, A.W. Sleight, J. Solid State Chem. 151 (2000) 323.
[10] C.C. Homes, T. Vogt, S.M. Shapiro, S. Wakimoto, A.P. Ramirez, Science 293 (2001) 673.
[11] P. Jha, P. Arora, A.K. Ganguli, Mater. Letts. 57 (2003) 2443.
[12] P. Jha, S. Bobev, G.N. Subbanna, A.K. Ganguli, Chem. Mater. 15 (2003) 2229.
[13] P. Jha, A.K. Ganguli, Proc. Ind. Acad. Sci. 115 (2003) 431.
[14] H. Asano, J. Hayakawa, M. Matsui, Phys. Rev. B 56 (1997) 5395.
[15] R. Laiko, K.G. Lisomov, E. Lahderanta, P.A. Petrensko, J. Salminen, V.N. Stamov, Y.P. Stepsnov, V.S. Zakhvalinskii, J. Phys. Chem. Solids 64 (2003) 2313.
[16] C. Himcinshi, E. Burzo, R. Tetean, D. Ristoiu, V. Pop, Mod. Phys. Lett. B 17 (2003) 263.
[17] R.-W. Li, Z.-H. Wang, X. Chen, J.-R. Sun, B.-G. Shen, J. Appl. Phys. 87 (2000) 5597.
[18] P. Selwood, Magnetochemistry, Interscience, New York, 1956.
[19] W.J. Zhu, Y.Z. Huang, T.S. Ning, Z.X. Zhao, Mater. Res. Bull. 30 (1995) 243.
[20] M.J. Pack, A. Gormezano, M.T. Weller, Chem. Mater. 9 (1997) 1547.
[21] C.D. Wagner, W.M. Riggs, L.E. Davies, J.F. Moulder, G.E. Muilenberg, Handbook of X-ray Photoelectron Spectroscopy, Perkin Elmer Corp., Minnesota, 1979.
[22] C.G. Koops, Phys. Rev. 83 (1951) 121.
[23] M.A. El Hiti, J. Magn. Magn. Mater. 192 (1999) 305.
[24] D. Ravinder, A.V. Ramanna Reddy, G. Ranga Mohan, Mater. Lett. 52 (2002) 259.
[25] A.R. West, Solid State Chemistry and its Applications, Wiley, New York, 1985.
[26] S.J. Youn, B.I. Min, Phys. Rev. B 56 (1997) 12046.
[27] B. Dabrowski, K. Rogacki, X. Xiong, P.W. Klamut, R. Dybzinski, J. Shaffer, J.D. Jorgensen, Phys. Rev. B 58 (1998) 2716.
[28] E.F. Bertaut, E.F. Forrat, P.H. Faug, Comput. Rend. 256 (1963) 1958.
[29] Z.J. Huang, Y. Cao, Y.Y. Sun, Y.Y. Xue, C.W. Chu, Phys. Rev. B 56 (1997) 2623.
[30] M. Fiebig, Th. Lottermoser, D. Fröhlich, A.V. Goltsev, R.V. Pisarev, Nature 419 (2002) 818.
[31] M.H. Whangbo, H.J. Koo, D. Dai, D. Jung, Inorg. Chem. 41 (2002) 21.
[32] Y.J. Wu, X.M. Chen, J. Mater. Res. 16 (2001) 1734.